

THESIS

INVESTIGATION OF STORAGE-PHOSPHOR AUTORADIOGRAPHY FOR ALPHA  
EMITTERS ON DIFFERENT TYPES OF FILTERS

Submitted by

Ashley Sorcic

Department of Environmental and Radiological Health Sciences

In partial fulfillment of the requirements

For the Degree of Master of Science

Colorado State University

Fort Collins, Colorado

Spring 2019

Master's Committee:

Advisor: Ralf Sudowe

Alexander Brandl  
Pinar Omur-Ozbek

Copyright by Ashley Sorcic 2019

All Rights Reserved

## ABSTRACT

### INVESTIGATION OF STORAGE-PHOSPHOR AUTORADIOGRAPHY FOR ALPHA EMITTERS ON DIFFERENT TYPES OF FILTERS

Numerous incidents in the past have resulted in the release of radioactive contamination into the environment, some of which require continuous monitoring decades later. Past and potential future incidents encourage governments and regulating agencies to develop procedures and methods to deal with nuclear emergencies, decontamination and decommissioning, and historical preservation in the face of a possibly dangerous environment. One technique which may assist in forensics and clean-up efforts is digital autoradiography. Digital autoradiography is based on the creation of luminescence due to the interaction of ionizing radiation with the storage phosphor. The resulting image can provide information about the amount and spatial distribution of the radioactivity in a sample. While the technique is typically used for the imaging of beta-emitting radionuclides, it can also be used for alpha emitters. Previous work has shown a correlation between the radioactivity of the sample and the intensity of the light emitted by the phosphor. In addition, it was observed that the luminosity varied for different alpha emitting isotopes. The current work extended this research to other alpha emitting isotopes and the effect of the energy of the emitted alpha particle on the response of the phosphor screens. In addition the effect of different types of air filters as source material was investigated, as well as the response of Multi-Sensitive storage phosphor screens compared to SuperResolution screens. The last major variable considered was how wrinkled the filters were; this variable was first considered shortly after the sample preparations were complete.

## ACKNOWLEDGEMENTS

I would like to take a moment to acknowledge those who supported me while I was working towards a Master's degree. First and foremost, I am grateful to my advisor, Dr. Ralf Sudowe, for being eternally patient and encouraging with me. I would also like to thank the other members of my committee, Dr. Alexander Brandl and Dr. Pinar Omur-Ozbek for their support and comments.

A special thanks goes to my classmates for dealing with me while I was writing, and for being supportive friends. Finally, I would like to thank my friends outside the program and my family for their continuous support and love. Thank you all for keeping me sane.

## TABLE OF CONTENTS

ABSTRACT.....	ii
ACKNOWLEDGEMENTS.....	iii
LIST OF TABLES.....	vi
LIST OF FIGURES .....	vii
1. CHAPTER 1 – INTRODUCTION.....	1
1.1 Forensics and Emergency Response.....	1
1.1.1. Radiological Incidents and Air Monitoring.....	1
1.1.2. Decontamination and Decommissioning.....	3
1.1.3. Current Analysis Methods .....	4
1.2 Autoradiography.....	5
1.2.1. History Overview.....	5
1.2.2. Storage Phosphor Mechanics.....	6
1.2.3. Dose and Reading.....	7
1.3 Literature Review.....	8
1.3.1. Current Use.....	8
1.3.2. Recent Studies.....	8
1.3.3. Background and Fading Effects.....	9
1.4 Scope of Work to be Performed.....	10
2. CHAPTER 2 – MATERIALS AND METHODOLOGY.....	11
2.1 Materials.....	11
2.2 Sample Preparation.....	11
2.2.1. Filtration Apparatus:.....	11
2.2.2. Microprecipitation:.....	12
2.3 Autoradiography.....	13
3. CHAPTER 3 – RESULTS.....	16
3.1 Sample Preparation.....	16
3.2 Activity Calibration Curves.....	17
3.3 Filter Analysis.....	22
4. CHAPTER 4 – DISCUSSION.....	24
4.1 Activity Calibration Curves.....	24
4.2 Filter Analysis.....	25
4.3 Error Analysis.....	27
5. CHAPTER 5 – CONCLUSION.....	30
5.1 Overview.....	30
5.2 Activity Calibration Curves.....	30
5.3 Filter Analysis.....	30
5.4 Film Comparison.....	31
5.5 Future Work.....	31
REFERENCES.....	33
APPENDIX A.....	36
A.1. Equipment.....	36
A.2. Chemicals & Radionuclides.....	36

APPENDIX B.....	37
APPENDIX C.....	39
CURRICULUM VITAE.....	45

## LIST OF TABLES

Table 1- Comparison between energy of isotope and slope of fitted line. ....	24
Table 2- Response, in DLU/mm <sup>2</sup> , of SR film to 150 Bq deposited onto each filter type.....	26
Table 3- Response, in DLU/mm <sup>2</sup> , of MS film to 150 Bq deposited onto each filter type.....	26
Table 4- Percent difference between the values recorded in Table 2 and Table 3. ....	26
Table 5- Percent difference.....	27
Table 6- Raw data for Figures 4, 8, and 10.....	39
Table 7- Raw data for Figures 7 and 10.....	40
Table 8- Raw data for Figures 9 and 10.....	40
Table 9- Raw data for Figure 11. ....	41
Table 10- Raw data for Figure 12. ....	43
Table 11- Raw data for Figure 13. ....	44

## LIST OF FIGURES

Figure 1- Filtration set-up. ....	12
Figure 2- A sample set on Resolve® filter prior to imaging. ....	14
Figure 3- A sample set on Nuclepore filters prior to imaging. ....	14
Figure 4- Comparison of response between four sample sets on Resolve® filters. ....	17
Figure 5- Output image of SR film exposed to Am-241 on Resolve® filters ....	18
Figure 6- Report generated by the OptiQuant image analysis software for the image in Figure 5. .....	18
Figure 7- The activity response of SR film for Am-241 samples on Resolve® filters.....	20
Figure 8- The activity response of SR film for Pu-239 samples on Resolve® filters. The smooth set is included in the image as a separate data set.....	20
Figure 9- The activity response of SR film for Cm-244 samples on Resolve® filters.....	21
Figure 10- Fitted lines for all isotopes on Resolve® filters imaged using SR film.....	21
Figure 11- Gathered data for isotopes on Resolve® filters imaged using MS film.....	22
Figure 12- SR film response to different filters by isotope. ....	23
Figure 13- MS film response to different filters by isotope.....	23
Figure 14- Comparison of smooth and wrinkled Resolve® filters holding Pu-239. Imaged using SR film.....	25
Figure 15- A sample set of Am-241 at various activities on Resolve® filters, image captured by SR film.....	27
Figure 16- OptiQuant software protocol prior to scanning.....	37
Figure 17- OptiQuant software protocol prior to generating the report output on one of the screens.....	38



# 1. CHAPTER 1 – INTRODUCTION

## **1.1 Forensics and Emergency Response**

In the past, large areas have been deemed unfit for habitation due to the amounts of radionuclides in the environment. In the decades following the discovery of radiation, a number of laboratories were contaminated enough that today it is considered dangerous to enter, and multiple radiological incidents have necessitated evacuation and continuous environmental monitoring, both throughout clean-up efforts and beyond. These incidents and locations have forced governments and regulating agencies to develop procedures and methods to deal with nuclear emergencies, decontamination and decommissioning, and historical preservation in the face of a potentially dangerous environment. In the first two cases, radiological monitoring is essential for assessing doses and risks to responders and local populations alike; in both decommissioning efforts and in the preservation of historical sites, assessing the precise locations of radionuclides as well as assessing doses and radiological risks are essential in best protecting workers and local populations. Proper management of all three cases requires a knowledge of the situation which is as timely and complete as possible.

### *1.1.1. Radiological Incidents and Air Monitoring*

Whether or not the release was intentional, many large-scale radiological incidents release airborne radionuclides. How and where a plume of radionuclides moves affects emergency measures, including evacuation, zone restriction and management, and decontamination efforts. Airborne releases can be modelled by sophisticated software, but must be quantified and tracked by aerial monitoring. At both high altitudes and at ground level, measurements are completed with air samplers and various radiation detectors.

Air monitoring is one part of a radiological assessment, which is defined as “the quantitative process of estimating the consequences to humans resulting from release of radionuclides in the biosphere.” (Eisenbud and Gessell, 1997) Essentially, a radiological assessment takes into account the transport of radionuclides through an ecosystem, uptake by humans, and the dose from that uptake in order to estimate risk due to the radiological part of an incident. Atmospheric transport is one possible method for radionuclides to spread from the epicenter of an incident, and provides three distinct hazards – via immersion in a radiation field, inhalation, or deposition of material onto food or water sources. Dispersion happens relatively quickly in good conditions, though a still day may result in a high concentration of contamination in one area, and any material that has settled may be resuspended into the atmosphere by wind, fire, or other means. Material carried via atmospheric transport can be measured using air sampling.

Air sampling is accomplished by drawing air through a sampling tube and a filter for a known period of time, which can range between hours and weeks, and at a known flow rate. An air sampling system contains a pump, a filter or other device to separate particulates from the air flow, and a device to measure the flow of air and how much of it has passed through the system. (Cember and Johnson, 2009) Filters in an air sampling system are typically glass fiber, cellulose, polystyrene, or a membrane. A variety of factors influence how effective a filter is in a particular situation, including the diameter of the particles to be trapped, the size of the pores in the filter which trap particles as air flows through, how well the filter retains trapped particles, the flow rate of air through the system, and the compatibility of the filter with the selected analysis method – for instance, some filters can be dissolved to suspend the trapped particles in a liquid medium, while others remain mainly unaffected by attempted dissolution methods.

Radioactive material may clump together into a small particle (~1 mm down to several  $\mu\text{m}$ ) known as a “hot particle.” (Charles and Harrison, 2007) Such particles impact the uniformity of the dose field, and their presence represents a risk of a high localized dose through skin contact, inhalation, or ingestion. Detecting and characterizing hot particles is an important part of determining the type of risk posed to workers in the area, the method of transport through the environment, and the ultimate fate of the particle. It has traditionally been difficult to map the spacial distribution of radioactivity on a filter sample due to the destructive nature of the most informative tests, therefore making the detection of hot particles difficult.

#### *1.1.2. Decontamination and Decommissioning*

NUREG-1757 offers guidance on the decommissioning of sites licensed to use nuclear material in the US. The document, published by the Nuclear Regulatory Commission (NRC), divides sites undergoing decommissioning into seven groups based on the location and amount of residual radioactivity, as well as the complexity of decommissioning activities. Ultimately, as stated in NUREG-1757, licensees of decommissioned sites should be able to demonstrate that the site in question meets the appropriate levels according to site-specific models. So long as it is appropriately sensitive, the detection method used to demonstrate compliance is considered unimportant; however, there are few available methods capable of testing for alpha or beta contamination, each with their own disadvantages. One that most methods share is a lack of localization ability, leading to some areas being needlessly decontaminated while others may have undetected contamination. The ability to nondestructively test for, and localize within a small margin, contamination would minimize the amount of nuclear waste from decommissioning efforts.

### *1.1.3. Current Analysis Methods*

Currently, isotopic analysis of low levels of alpha activity is typically completed using alpha spectrometry techniques. Once an air sampler filter is dissolved, the resulting solution is separated for analysis based on selected radioelement. Isolating the analytes of interest from the solution requires both chemical and physical processes, of which chromatographic or ion exchange resins are a known and dependable partitioning method, though total separation depends on the sample and may require hours to weeks in order to complete. After successful separation, the sample can then be prepared for alpha spectrometry, using one of three procedures: electrodeposition, evaporation, or microprecipitation.

Solid-state detectors usually consist of a silicon charged-particle plate and an air-tight chamber in which the sample is placed prior to the chamber being evacuated. Charged particles from the sample being measured strike the silicon semiconductor and knock out an electron, forming an electron-hole pair and generating a detectable charge, which is collected and read by the electronics attached to the detector. The number of electron-hole pairs generated, each requiring 3.6 eV during generation, by an alpha particle interacting with the silicon semiconductor allows the computer system linked to the detector to calculate the energy of each individual particle and construct a spectrum unique to each isotope. (Knoll, 2000) In order to minimize statistical uncertainty on low-level samples, alpha spectrometry utilizes long count times, which is counterproductive when an analysis needs to be completed rapidly, as in the case of emergency operations. In addition, the technique is a method of destructive testing, requiring the sample to be completely dissolved during pre-test preparation, contrary to the needs of historical preservation efforts.

A second, non-destructive option for alpha analysis is swipe testing. Traditionally used to measure beta contamination, swipes may also provide information about the activity of alpha contamination in an area. They are, however, fairly limited – only removable contamination is detectable, and small, random samples are expected to represent large areas. (ISO standards, 1988)

## **1.2 Autoradiography**

Overall, autoradiography is a technique similar to film photography, in that it uses a special screen or plate to record an “image” of an object over some amount of time. The intensity of the recorded image depends on the amount of “light” emitted from the object being “pictured,” just as the image intensity of a photograph depends on how much light reflects off the object as it is being pictured. The images can be obtained and developed rapidly in comparison to alpha spectroscopy, and may prove useful in expediting alpha analysis in emergency situations where speed is especially desirable and in situations where destructive testing is undesirable, as in restoration and decontamination efforts. Despite a lack of sensitivity compared to alpha spectrometry, autoradiography could provide a dose estimate and greater information about the special distribution of the radioactivity present in the testing sample.

### *1.2.1. History Overview*

The first recording medium for radiography was a plate made of silver halide. As early as the mid-1800’s scientists noted that certain materials left developable images on silver halide plates, even when pieces of colored paper were between the source and the plate. However, the scientists who observed these effects concluded that the images left on the plates were due to luminescence, a known phenomenon where visible light is emitted by a sample. Radioactivity was first identified and described as a new and unknown process when Henri Becquerel observed

images left on photographic film stored in complete darkness next to uranyl sulfate salts.

(Yagoda, 1949) The realization that the effect was tied to the uranium in the compound led to a series of studies using photographic film and different materials. From those studies, scientists noted that a sample always formed the same image, allowing the localization of radioactive particles and identification of new elements.

Over time, the techniques used in autoradiography have changed and improved as various uses have demanded better resolution, faster imaging, or greater sensitivity to lower amounts of radioactivity, among other possible requirements. Silver halide films with extremely fine grain are able to provide the best resolution for detailed images, but most modern autoradiography is performed by creating digital scans of storage phosphor screens. Storage phosphor technology initially grew from a Fujifilm-developed alternative to diagnostic radiography X-ray film released in the early 1980s. (Parsons-Davis et al, 2018)

### *1.2.2. Storage Phosphor Mechanics*

The basic mechanism behind a storage phosphor is the same mechanism behind scintillation detectors. In a scintillator, energy from radiation is absorbed, then transferred to a waveshifter which emits that energy as a wavelength detectable by a photomultiplier tube (PMT), which then sends a signal to a computer. A storage phosphor is a little different, however, in that the energy is stored and the material must be stimulated in order to release detectable energy in the form of blue light.

In phosphor imaging, a layer of barium fluorohalide crystals doped with europium store energy transferred into the material from radiation. The image is stored by oxidation of europium, from  $\text{Eu}^{2+}$  to  $\text{Eu}^{3+}$ , and by trapping the promoted electrons in matrix vacancies. Shining a laser on the material stimulates the trapped electrons, allowing the reduction of the

europium back to  $\text{Eu}^{2+}$  and releasing characteristic light which is then detected with a photomultiplier tube. The output signal from the photomultiplier tube is digitally constructed into an image of the dose absorbed by the storage phosphor at every individually scanned point. The resolution of the image depends on the same factors which film resolution is contingent on – emulsion thickness, grain size, the readout system, and the properties of the imaged sample. (Parsons-Davis et al, 2018; Johnston et al, 1990; Upham and Englert, 1998)

### *1.2.3. Dose and Reading*

“Dose” refers to the amount of energy absorbed when an object, living or not, is exposed to radiation. Aside from solid sources external to a body, in many unusual situations there may be airborne radioactive particles small enough to be inhaled, or food and drink may become contaminated and provide another pathway for radioactive materials to enter a body. Once inside, the radiological and biological half-lives of the elements that have been inhaled or ingested determine how long the elements stay in the body, while radiation type and energy determine what effects and damages the body sustains. Alpha radiation in particular is a much larger concern for internal exposure than for external, and a much larger concern than other types of radiation due to a much higher biological effectiveness arising from a larger size and higher linear energy transfer (LET) than other types of radiation. This higher biological effect and the greater risk associated with airborne alpha-emitting isotopes means that, in cases where airborne contamination is a significant risk, filters from air monitors are typically examined via alpha spectroscopy after other non-destructive testing, such as proportional counting.

As the storage phosphor absorbs a greater dose, the energy released in the form of detectable light after laser stimulation increases. In many cases the dose response of storage phosphor screens has previously been shown to be linear if all other factors are the same. (Knol

et al, 2008) However, the detection efficiency, sensitivity, and resolution may vary depending on the imaged isotopes, and signal fade begins to affect the stored image almost immediately upon exposure to any source of light or if the time between exposure and image development is more than a few days.

### **1.3 Literature Review**

#### *1.3.1. Current Use*

Autoradiography techniques have a wide variety of accepted uses, stemming from a relatively long history as well as the qualitative and semi-quantitative nature of the method. With the capability to view the special distribution of radioactivity, autoradiography is a popular method in life sciences to identify locations of tagged proteins in order to track various biological functions, as well as in monitoring materials near reactors for potential activation, mapping low levels of uranium and thorium in minerals, and in measuring beam profiles. Most often, autoradiography is used primarily or solely to observe the distribution of radioactivity in samples, though there are ongoing studies investigating the use of autoradiography in quantifying radioactive samples. Interest in quantitative uses of autoradiography primarily stem from the main advantages of the method – detection of special distribution in radioactive samples, and short required exposure times even for low-activity samples.

#### *1.3.2. Recent Studies*

Recent studies focusing on autoradiography and storage phosphor imaging tend to investigate quantitative uses for the technology, as well as forensic uses, the effects of fading and other environmental factors on image quality.



Mori and Matsumura examined the sensitivity of storage phosphor screens to alpha particles; they found that storage phosphor screens are sensitive to alpha radiation emitted by Pu particles, even through four sheets of Mylar film. (Mori et al, 1994)

Ang et al and Molteni investigated various fading effects, specifically using versions of storage phosphor imaging and software developed for dental needs. (Ang et al, 2006; Molteni, 2003)

Gallardo investigated storage-phosphor autoradiography for the use of quantitatively screening air filters in emergency situations. (Gallardo, 2013)

Parsons-Davis et al investigated the usefulness of digital autoradiography and storage phosphor in the context of nuclear forensics. They specifically concentrated on identifying areas of interest during routine screening of nuclear material for later micro-characterization. (Parsons-Davis et al, 2018)

### *1.3.3. Background and Fading Effects*

Ang et al investigated the effect of time-based fading on three aspects of dental images taken with phosphor imaging plates. (Ang et al, 2006) Forty-eight storage phosphor images of the chosen sample were obtained, then scanned immediately or after an amount of time – 1 hour, 8 hours, 24 hours, 72 hours, or 168 hours. Prior to scanning, all phosphor screens were stored in a light-tight black box, so the only variable tested was the length of time between exposure and scanning. With regards to diagnostic image quality and spatial resolution, the investigators found no significant difference, possibly due to the software used in the study. However, after 24 hours there was a significant difference in the average pixel intensity – that is, the brightness of the luminescence detected from the stimulated storage phosphor decreased significantly.

Molteni quantitatively investigated the effect of light exposure on storage phosphor plates, with the purpose of establishing proper guidelines for handling imaging plates prior to scanning and during erasure. (Molteni, 2003) The experiment examined signal loss from a storage phosphor under different lighting conditions, including under an incandescent bulb and various types of fluorescent bulbs. The conclusion of the experiment notes that most of the signal loss occurs within the first 10 seconds of exposure for all types of lights used; further, the signal loss follows an exponential decay, with some residual signal remaining long after the first minute of erasure.

#### **1.4 Scope of Work to be Performed**

The objective of this research is to develop an efficient, non-destructive method of visualizing and quantifying alpha-emitting contamination located on or moved to a filter, as in air samples taken from the aftermath of a contamination-release event, swipe samples, or other samples which can be microprecipitated onto an appropriate filter. The nuclides of interest in this study are Am-241, Pu-239, and Cm-244, which are common reactor products and may be used in industry and research. Various activities of each isotope will be microprecipitated onto filters, then one activity of each isotope will be microprecipitated onto various types of filters. The samples will be analyzed and imaged using autoradiography. Calibration curves for each isotope will be constructed and comparisons will be made between different filter types. There are three types of storage phosphor imaging films that have been categorized based on sensitivity to beta emitters. Two types of film, MultiSensitive (MS) and SuperResolution (SR), will be used to image the samples in this work.

## 2. CHAPTER 2 – MATERIALS AND METHODOLOGY

### 2.1 Materials

A full list of materials is located in Appendix A.

### 2.2 Sample Preparation

Samples with different activities were prepared for microprecipitation. The PAL Lifescience apparatus, in conjunction with a vacuum pump, was used to filter the samples one at a time. Filters were positioned in the apparatus by removing the plastic funnel, placing the filter on top of the screen, and replacing the funnel. Filters were conditioned for microprecipitation, and a leak test performed each time the funnel was replaced, by adding 3-5 mL of 80% ethanol to the funnel and passing the liquid through under vacuum, then rinsing the filter with 2-3 mL of deionized water (DI).

#### 2.2.1. *Filtration Apparatus:*

A filtration apparatus consisting of a PAL Lifescience filter holder with polycarbonate base and metal screen, 25 mm polysulfone funnel, and 250 mL polypropylene flask were used to filter one sample at a time. The filters used all had a pore size of 0.1  $\mu\text{m}$  and a diameter of 25 mm, though the material varied. The activity calibration curve, and the largest set of samples, was microprecipitated onto Eichrom Resolve® polypropylene filters. Filters were placed on the metal support screen, which the polysulfone funnel screwed on overtop to lock the filters in

place. The flask was connected through another, identical flask, which served as a buffer, to a vacuum pump. The full set-up is shown in Figure 1- Filtration set-up..

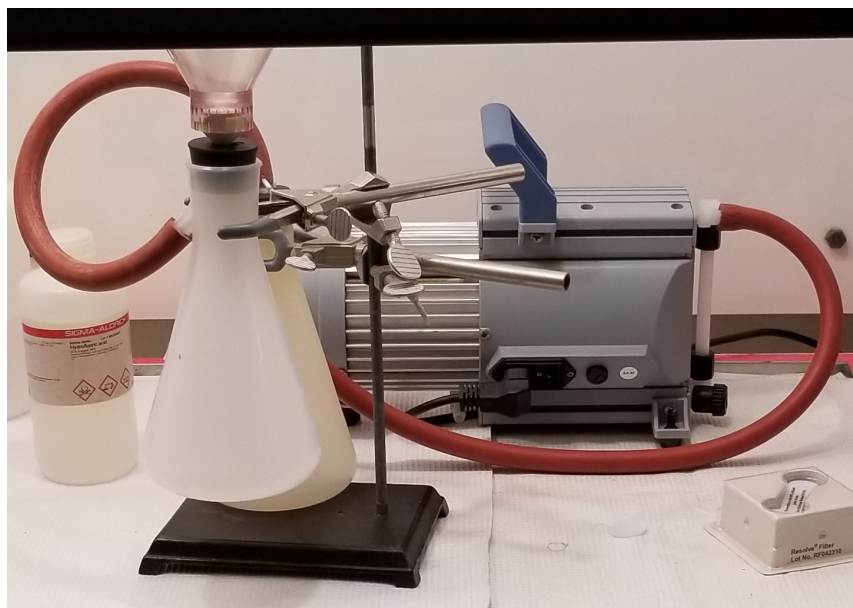


*Figure 1- Filtration set-up.*

### *2.2.2. Microprecipitation:*

A cerium fluoride microprecipitation procedure was used to create the samples. First, to about 4 mL of 0.1 M nitric acid in a 15 mL centrifuge tube, a predetermined amount of analyte was added before enough 0.1 M nitric acid was added to bring the total sample volume to 5 mL. Then, 0.1 mL of a cerium carrier (0.5 mg/mL Ce as  $\text{Ce}(\text{NO}_3)_3$ ) was mixed into each of the samples prior to adding 1.0 mL of concentrated hydrofluoric acid. The solutions were swirled and allowed to sit for 30 minutes before filtration. The filters were prepared immediately prior to filtration using several drops of 80% ethanol, to open the filter pores, then DI while applying a vacuum. While filtering a sample, the centrifuge tube which had contained it was rinsed with DI, then that rinse was filtered as well. The process finished with rinsing the filter using 3-5 mL of 80% ethanol to replace any water remaining in the filter pores. The sample was then removed

and placed it under a heat lamp for a few minutes to dry. Samples produced by this process contained 50, 100, 150, 200, or 250 Bq of Am-241, Pu-239, or Cm-244.

### **2.3 Autoradiography**

The filters, prior to drying in the case of the Resolve® and after drying for the others, were mounted to stainless steel planchets using double-sided tape, then stored in covered petri dishes. The Perkin Elmer storage phosphor system and OptiQuant software were used to gather data on the various samples. When imaging, the samples were arranged in the exposure cassette in a pattern such that the location of each sample is obvious on the scanned images. The cassette held the samples tightly against the storage phosphor film during the exposure process. The phosphor itself had been photobleached prior to placement in the cassette, which meant any previous signal still remaining was erased by exposure to a bright white light. (Perkin Elmer Inc., 2006) Figure 2- A sample set on Resolve® filter prior to imaging. shows the layout of the samples on Resolve® filters in a light-tight exposure cassette, and Figure 3- A sample set on Nuclepore filters prior to imaging. shows the layout of the samples microprecipitated onto other filters. Each set of samples was exposed for 2.5 hours and imaged in groups according to filter type and isotope.



*Figure 2- A sample set on Resolve® filter prior to imaging.*



*Figure 3- A sample set on Nuclepore filters prior to imaging.*

After exposing the storage phosphor screens to the samples for an appropriate amount of time, the screens were removed from the exposure cassettes and placed in the carousel of the Cyclone Plus Storage Phosphor System for scanning. As an overview, during scanning the carousel rotates while a laser stimulates the storage phosphor and a PMT detects and magnifies the emitted luminescence. The signal from the PMT is converted into a digital output which can be read and analyzed by the OptiQuant software.

## 3. CHAPTER 3 – RESULTS

### 3.1 Sample Preparation

The filter samples were prepared according to the methods outlined in chapter 2. It was noted from the initial samples that taping the filters to the planchets prior to placing them under the heat lamp caused varying degrees of wrinkling in the filters as the tape shrank. A slight procedural change was therefore made after completing the microprecipitation of the three replicates of each isotope onto Resolve® filters – instead of taping the filters prior to drying, the filters were first dried, then taped. However, the cellulose nitrate filters wrinkled regardless of when the tape was applied. In order to examine the possible effects of wrinkled filter on the observed response, a set of smooth filters was selected out of all filters in the three Pu-on-Resolve® sets and compared to data for the wrinkled filters. The comparison was conducted on the Pu-239 sample sets because those sample sets displayed the greatest amount of wrinkling of all sets on Resolve® filters. Figure 4- Comparison of response between four sample sets on Resolve® filters. is a comparison of the SR film response to the three sets of Pu-239 on Resolve® filters and the set of smooth filters selected for assessment, normalized to the listed activities.



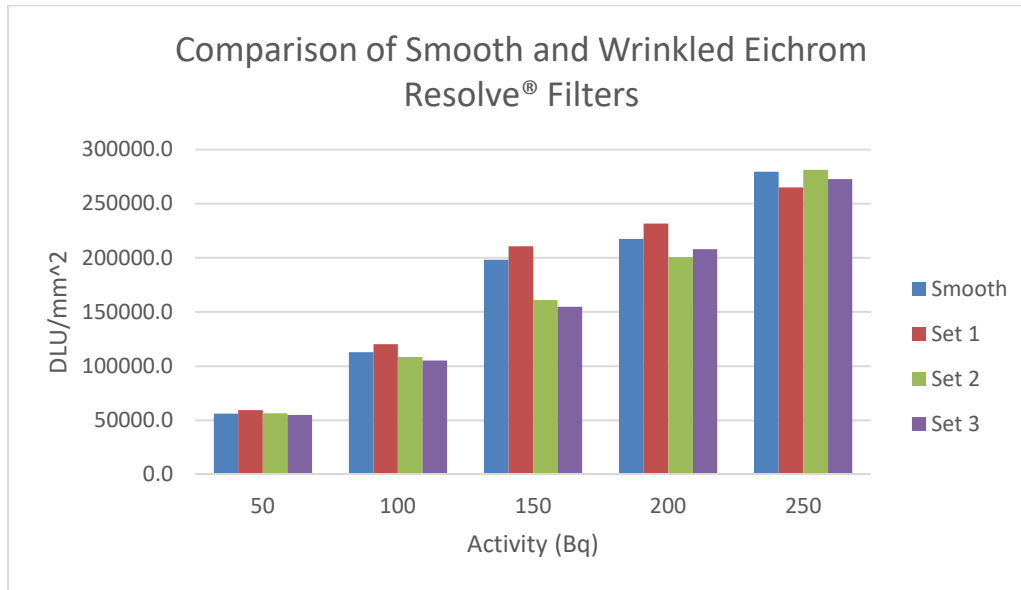


Figure 4- Comparison of response between four sample sets on Resolve® filters.

### 3.2 Activity Calibration Curves

A region with diameter of 25 mm, the same size as the filters and therefore of the region of interest (ROI), was scanned at 300 dpi, corresponding to 85 mm pixels. The OptiQuant software used to analyze the storage phosphor screens calculated the digital lights units (DLU) from each ROI, then included those values in an automatically-generated report. Reported DLUs are the sum of the intensity units in all the pixels within the ROI (Perkin Elmer Inc., 2006).

Figure 5- Output image of SR film exposed to Am-241 on Resolve® filters shows the OptiQuant output on SR film for one of the Am-241 sample sets on Resolve® filters. The colors in the image indicate the relative response, with red being a higher recorded response and blue being a lower recorded response. The color scale is adjustable and automatically scales to show the greatest amount of contrast within the scan. Along the left side of the image, the 50 Bq sample in the set has a lower density of blue pixels than the 100 Bq sample, indicating a lower response.

Figure 6- Report generated by the OptiQuant image analysis software for the image in Figure 5- Output image of SR film exposed to Am-241 on Resolve® filters. is an example of the “Report”

function output, giving the total DLUs in each selected region, the area of each region, and the intensity in DLU/mm<sup>2</sup>, among other values.

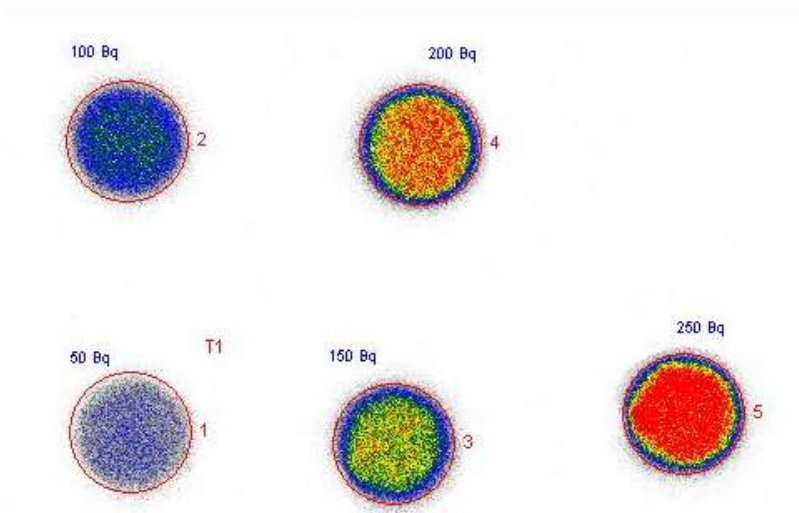


Figure 5- Output image of SR film exposed to Am-241 on Resolve® filters

File : Am241SRScreenA2.5hrSet1.tif Acquired : 11/2/2018 11:46:52 AM  
 Owner : User1 Subject : Am241, 2.5 hours, SR screen A  
 #T1 - Region Group

ID	Area(mm2)	Gross DLU	DLU /mm2	% Sum	% Max Reg	% Total
1 - EII	490.9	45,962,267.8	93,633.6	6.8	20.9	6.5
2 - EII	490.9	90,694,090.9	184,760.5	13.4	41.3	12.8
3 - EII	490.9	137,389,734.8	279,888.1	20.3	62.6	19.4
4 - EII	490.9	182,160,814.7	371,095.0	27.0	83.0	25.7
5 - EII	490.9	219,486,659.3	447,134.6	32.5	100.0	31.0
<b>Total</b>	31,172.9	707,882,173.5	22,708.3			100.0
<b>UnRes</b>	28,718.5	32,188,606.1	1,120.8			4.5

Figure 6- Report generated by the OptiQuant image analysis software for the image in Figure 5- Output image of SR film exposed to Am-241 on Resolve® filters.

Analysis of the data included a comparison between the recorded response to each isotope at each activity and a separate comparison between heavily wrinkled and smooth Resolve® filters. When plotted, the activity response for each isotope fit the expected trends

between slope and energy of the emitted alpha radiation, with Cm-244 having both the greatest slope and greatest alpha energy, and Pu-239 having the least. The data for each image was recorded, and each data point was graphed. Figure 7- The activity response of SR film for Am-241 samples on Resolve® filters shows the graph of the data collected after imaging all sets of Am-241 on Resolve® filters. Figure 8- The activity response of SR film for Pu-239 samples on Resolve® filters. The smooth set is included in the image as a separate data set. is the data from the Pu-239 sets, including the smooth set for comparison. Figure 9- The activity response of SR film for Cm-244 samples on Resolve® filters. displays the data from the Cm-244 sets, and Figure 10- Fitted lines for all isotopes on Resolve® filters imaged using SR film. depicts an overall comparison between the radionuclides using lines fitted for each. The same sample sets were imaged using MS film, with the results displayed in Figure 11- Gathered data for isotopes on Resolve® filters imaged using MS film.. While the MS film displays a lesser response than the SR film, indicated by smaller slopes in the fitted lines, the difference is generally negligible at the activity levels studied. In addition, the MS film displayed a smaller variability than the SR film; the sample standard deviation of the SR film was up to 15 times greater than the same value for the MS film. On average, the standard deviation of the SR film was 4.8 times greater than that of the MS film.

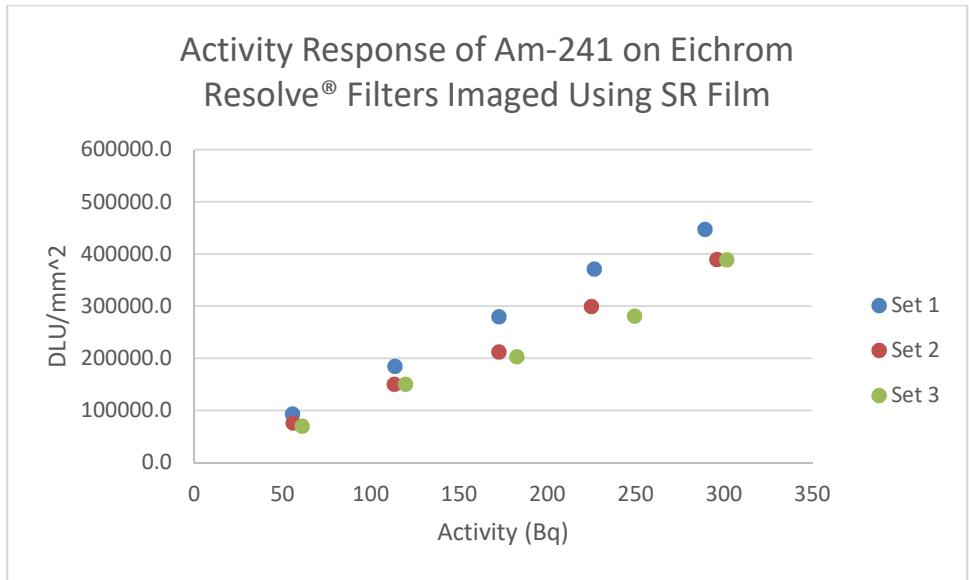


Figure 7- The activity response of SR film for Am-241 samples on Resolve® filters

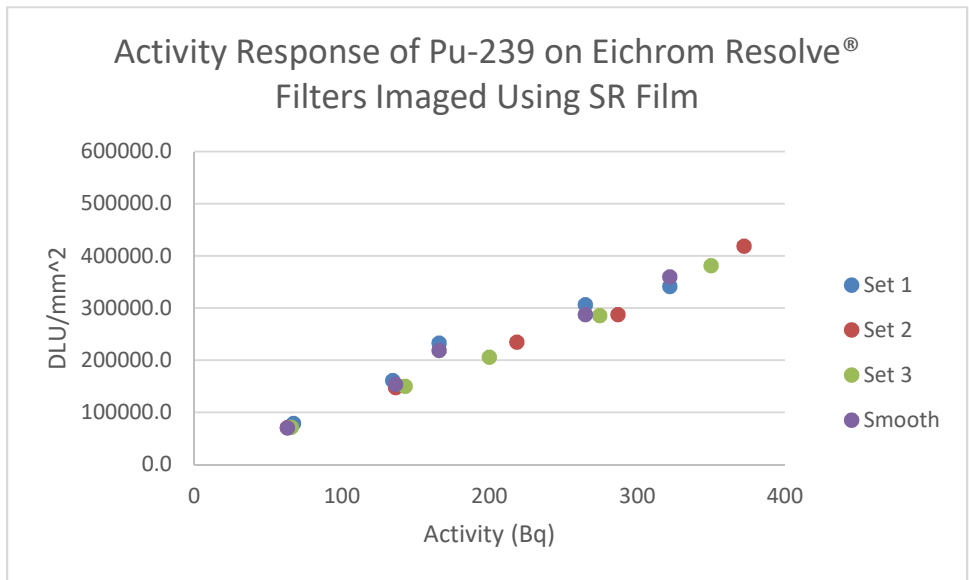


Figure 8- The activity response of SR film for Pu-239 samples on Resolve® filters. The smooth set is included in the image as a separate data set.

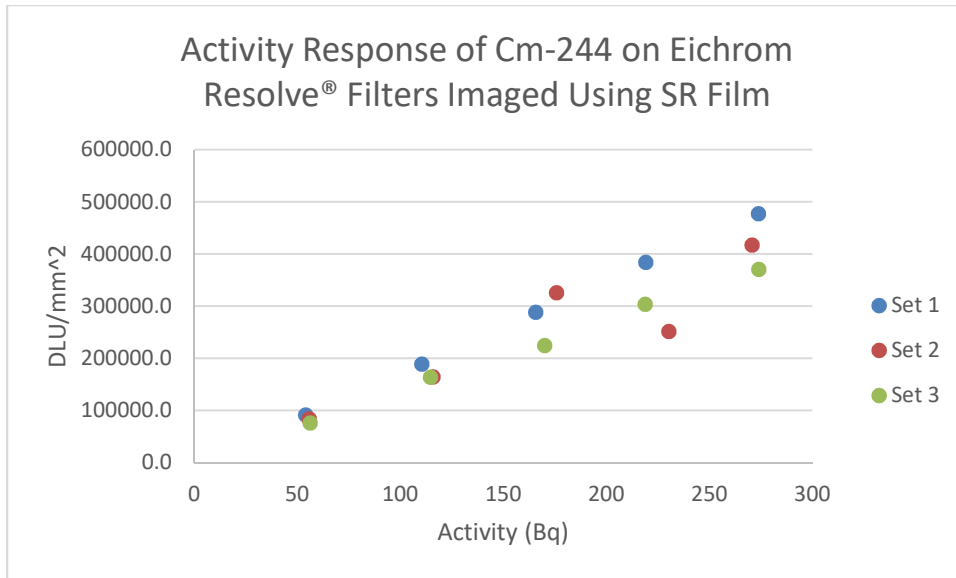


Figure 9- The activity response of SR film for Cm-244 samples on Resolve® filters.

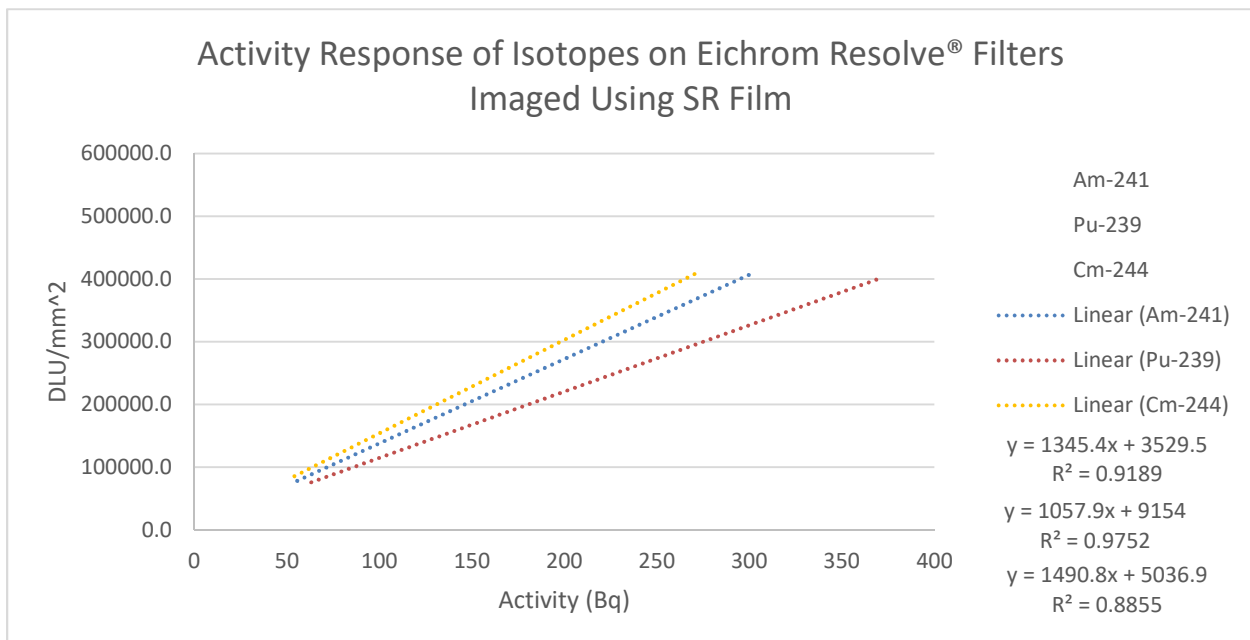


Figure 10- Fitted lines for all isotopes on Resolve® filters imaged using SR film.

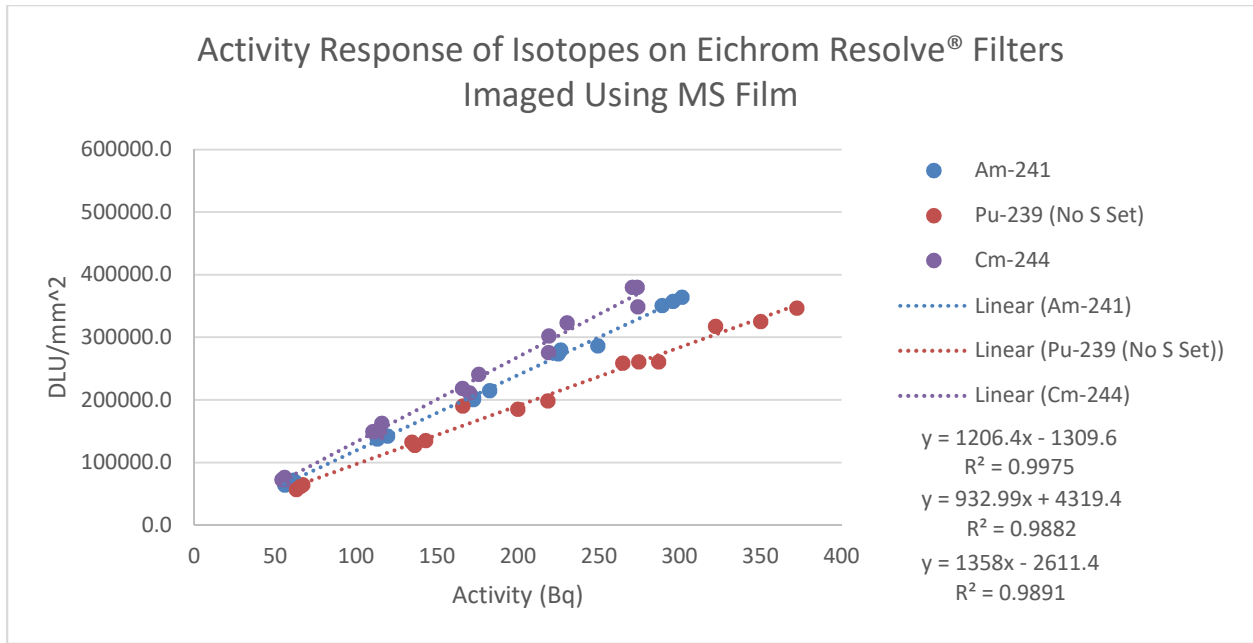


Figure 11- Gathered data for isotopes on Resolve® filters imaged using MS film.

### 3.3 Filter Analysis

Exposure to each of the three types of filters tested caused different levels of response from the storage phosphor screens. Overall, the screens had the greatest response to the Resolve® filters, and the lowest response to both the Nuclepore filters and the cellulose nitrate filters. In every case, the storage phosphor screens had the greatest response to Cm-244 and the lowest response to Pu-239. Figure 12- SR film response to different filters by isotope. and Figure 13- MS film response to different filters by isotope. display the responses of SR and MS films to each isotope on each type of filter, normalized to an activity of 150 Bq. In the case of data from the Resolve® filter sets, only the data from the samples where the intended activity was 150 Bq was considered for comparison purposes.

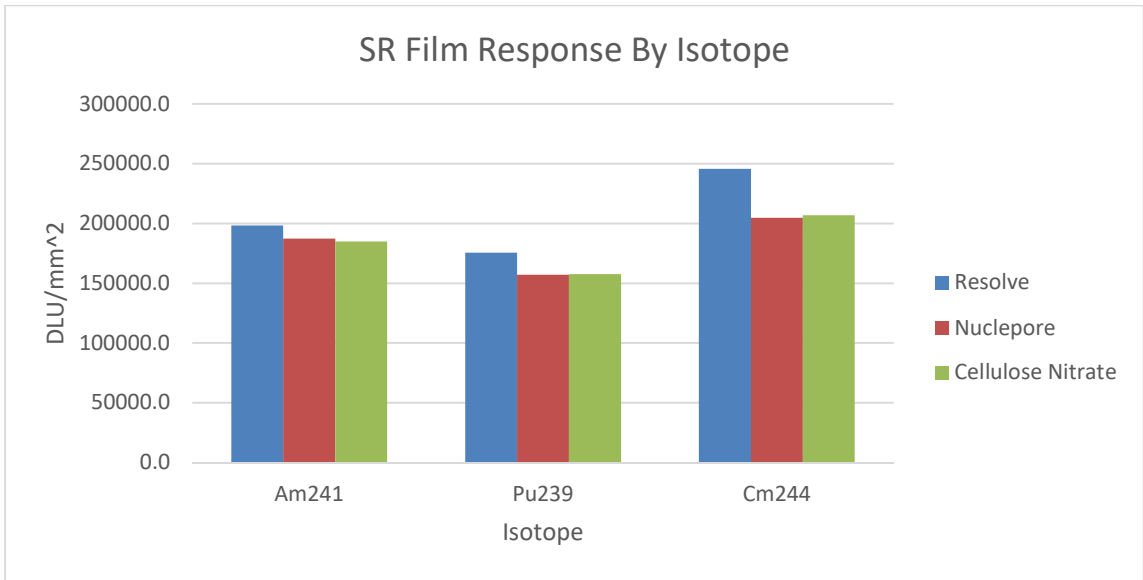


Figure 12- SR film response to different filters by isotope.

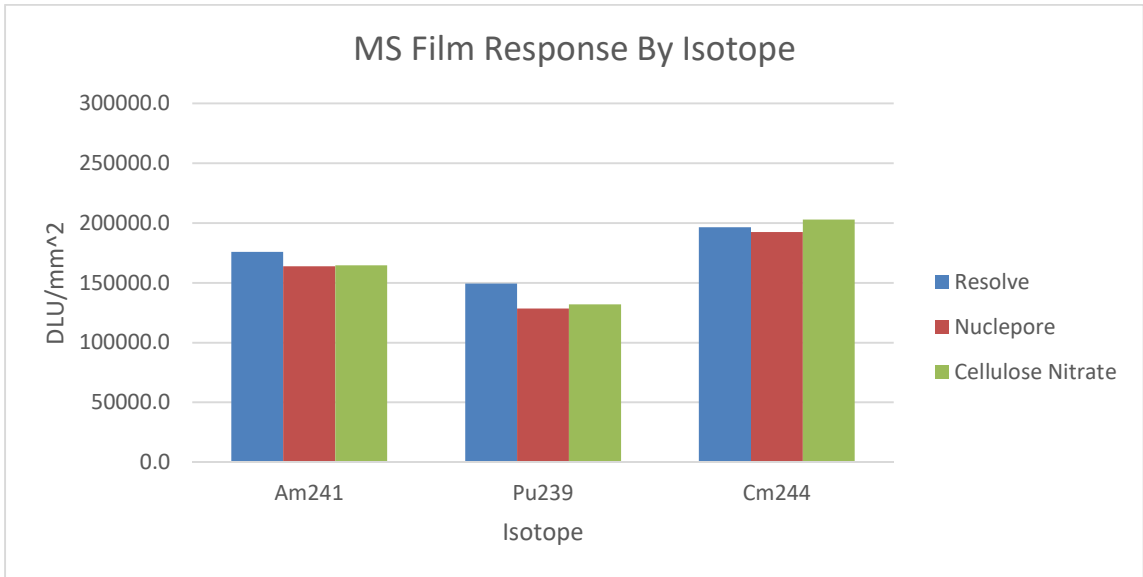


Figure 13- MS film response to different filters by isotope.

## 4. CHAPTER 4 – DISCUSSION

### 4.1 Activity Calibration Curves

The calibration curves generated for each isotope show a linear relationship between the activity of radioactivity deposited on the filters and the response of the storage phosphor in DLU/mm<sup>2</sup>. The slope of the relationship appears to correlate with the energy of the emitted alpha particle – with Cm-244 having both the highest alpha energy at 5.8 MeV and the greatest slope when compared to the other isotopes. Table 1- Comparison between energy of isotope and slope of fitted line. lists the isotopes used in order of decreasing energy of the emitted alpha particle, with the slopes of the fitted lines included in the table. From this data, it can be concluded that the energy of the emitted alpha particle has an effect on the slope of the fitted line – namely, that a higher energy results in a greater slope.

*Table 1- Comparison between energy of isotope and slope of fitted line.*

Isotope	Alpha Energy (MeV)	Slope of SR Fitted Line	Slope of MS Fitted Line
Cm-244	5.80	1490.8	1358
Am-241	5.48	1345.4	1206.4
Pu-239	5.15	1057.9	932.99

The linearity of the response, at the activity levels used in this experiment, does not appear to be significantly affected by how smooth or wrinkled the filters are, as determined by a statistical test for the difference between two sets of data which differed only in the smoothness of the filter surface. Figure 14- Comparison of smooth and wrinkled Resolve® filters holding



Pu-239. Imaged using SR film. is a graph of the different sets of Resolve® filters containing Pu-239, including the smooth set, for a visual comparison of how wrinkles in a filter set affected the imaging data.

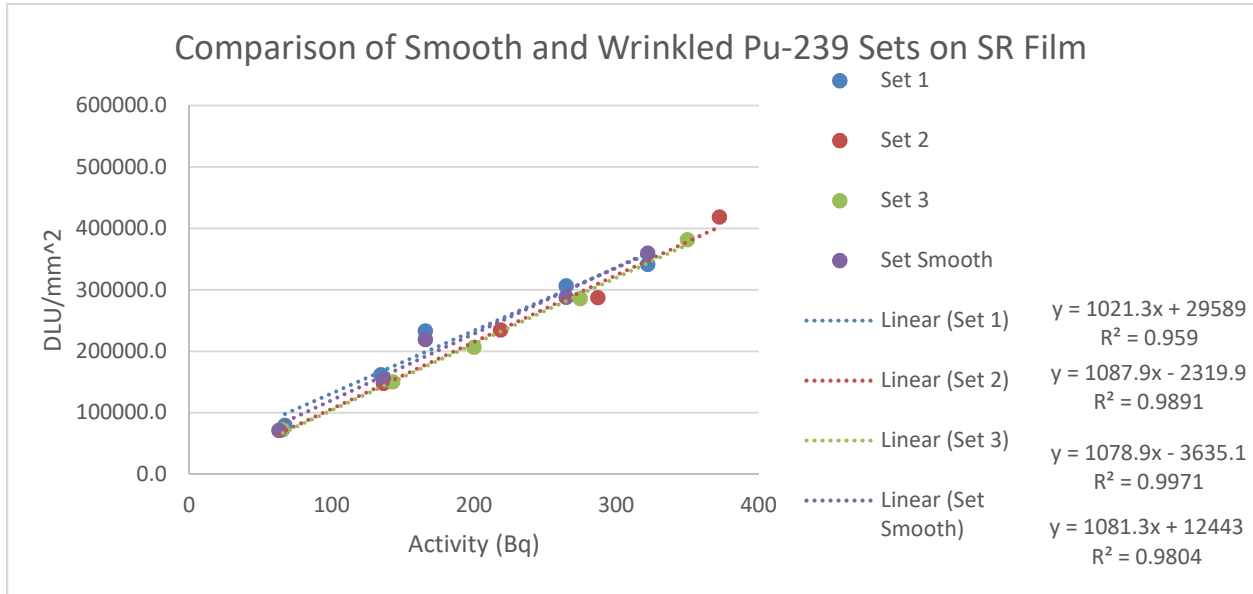


Figure 14- Comparison of smooth and wrinkled Resolve® filters holding Pu-239. Imaged using SR film.

## 4.2 Filter Analysis

In general, across all tested isotopes, the response was greatest for the Resolve® filters, with the Nuclepore and cellulose nitrate filters being comparable with each other. The recorded DLU/mm<sup>2</sup> for Cm-244 on Nuclepore filters was 16.7% smaller than the same activity and isotope on Resolve® filters, which was the greatest difference between the filter sets exposed to SR film. For Am-241 and Pu-239, the differences remained comparable regardless of whether SR or MS screens were exposed. The differences when Cm-244 was exposed decreased by an order of magnitude when the exposure was switched from SR screens to MS screens. Table 2 and

Table 3 list the response, normalized to 150 Bq, in DLU/mm<sup>2</sup> of SR and MS film, respectively, to each of the isotopes.

Table 4 is the calculated percent difference between the SR and the MS films, using the SR film as the baseline for comparison.

Table 5 lists the percent difference between filter sets, using the Resolve filters as the basis for comparison.

*Table 2- Response, in DLU/mm<sup>2</sup>, of SR film to 150 Bq deposited onto each filter type.*

SR film			
Isotope	Resolve	Nuclepore	Cellulose nitrate
Cm-244	245637.8	204724.7	206767.3
Am-241	198211.4	187399.2	185061.2
Pu-239	175602.2	157065.9	157558.1

*Table 3- Response, in DLU/mm<sup>2</sup>, of MS film to 150 Bq deposited onto each filter type.*

MS film			
Isotope	Resolve	Nuclepore	Cellulose nitrate
Cm-244	196522.0	192436.6	202928.6
Am-241	175958.4	163945.1	164674.7
Pu-239	149290.1	128450.2	131922.6

*Table 4- Percent difference between the values recorded in Table 2- Response, in DLU/mm<sup>2</sup>, of SR film to 150 Bq deposited onto each filter type. and*

*Table 3- Response, in DLU/mm<sup>2</sup>, of MS film to 150 Bq deposited onto each filter type.*

Percent difference			
Isotope	Resolve	Nuclepore	Cellulose nitrate
Cm-244	20.00	6.00	1.86
Am-241	11.23	12.52	11.02
Pu-239	14.98	18.22	16.27

Table 5- Percent difference

Percent difference from Resolve filters				
Isotope	Nuclepore, SR	Cellulose nitrate, SR	Nuclepore, MS	Cellulose nitrate, MS
Cm-244	-16.66	-15.82	-2.08	3.26
Am-241	-5.45	-6.63	-6.83	-6.41
Pu-239	0.00051	-10.28	0.00058	-11.63

### 4.3 Error Analysis

Errors could have been introduced during the sample production procedure, as uncertainties were. Microprecipitation was used to create thin, evenly-distributed samples that would present a clean image on storage phosphor screens. Some of the filters became wrinkled at different parts of the procedure, introducing areas where the recorded intensity was greater than it otherwise would have been. Figure 15 is an image of a sample set containing Am-241 at various activities captured on SR film, where some of the Resolve® filters in the sample set were wrinkled while under the heat lamp and others stayed smooth.

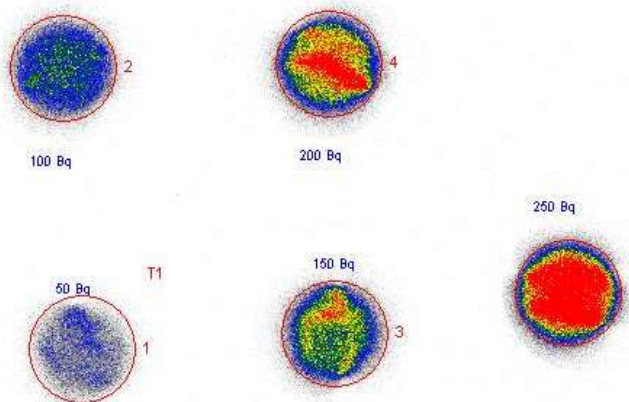


Figure 15- A sample set of Am-241 at various activities on Resolve® filters, image captured by SR film.

During sample preparation, a slight change was made after preparing the samples on Resolve® filters in response to a noticed problem. When the filters were taped to a planchet, then placed under a heat lamp to dry, the tape tended to shrink, leading to wrinkles in the filter. In subsequent sample sets, samples were taped to the planchets after being dried. In order to determine whether wrinkles made a significant difference in collected data, two special sample sets were selected out of the Pu-239 replicate sets, with one set being highly wrinkled and the other being completely or nearly-completely smooth. Data was collected for the two sets in the same manner as for all other sets, then compared using a statistical test in R in order to determine whether there was a significant difference between the two sets. At the activity levels used, the program reported no significant difference.

Ethanol was omitted while preparing the samples on Nuclepore filters. When preparing the first Nuclepore sample, it was noted that the vacuum pump was having trouble pulling liquid through the filter. Omitting the ethanol in the procedure increased the flow rate through the filter and did not appear to have any significant effect on how much analyte was retained by the filter – the deviation between the first Nuclepore sample and the second was less than 7%, which is an insignificant difference. The purpose of the ethanol was to open the pores of the Resolve filters and allow the sample to flow through the filter. The same process is unnecessary with Nuclepore filters, and even clogged the filter instead.

Error may also arise from conditions around the exposure itself. The film can be affected by any additional sources placed nearby during exposure, and background appeared to be higher inside the exposure cassette than outside. In addition, the film images may be impacted by the transfer from the light-tight exposure cassette to the scanning carousel, despite the transfer occurring in as dark a room as practical. The uncertainty associated with the storage phosphor

screens and the Cyclone Plus Storage Phosphor System are unknown and therefore the data cannot be adjusted to account for intrinsic uncertainty.

The size of the region of interest (ROI) used on the imaging phosphor to gather data may also contribute to error. The size of the ROIs was matched to the size of the filters – 25 mm. As such, not all of the DLUs generated by the samples may have fallen within the ROIs.

Error was also introduced during sample preparation. An automatic pipette was used to deliver the desired amount of activity to each sample solution. Using the pipette to transfer microliters of stock solution resulted in a range of actual activities in each sample. When determining the actual activity each sample filter contained, an alpha spectrometer was used to determine the time it took to reach 10000 counts. The number of counts used to determine the actual activity of each sample allowed accurate plotting of the response of the storage phosphor films in  $\text{DLU}/\text{mm}^2$  to the actual sample activities.

## 5. CHAPTER 5 – CONCLUSION

### 5.1 Overview

The use of digital autoradiography employing storage phosphors for the rapid localization and quantification of alpha-emitting isotopes was investigated. The difference in behavior of SuperResolution (SR) and MultiSensitive (MS) storage phosphor screens was also investigated, and it was determined that SR screens are more sensitive in terms of recorded DLUs per sample. The films were exposed for 2.5 hours to various sets of microprecipitated samples and scanned using the Cyclone Plus Storage Phosphor Scanner and OptiQuant analysis software. Calibration curves were generated based on Digital Light Units per unit area (DLU/mm<sup>2</sup>) and sample activities.

### 5.2 Activity Calibration Curves

The response of the storage phosphor films measured in DLU/mm<sup>2</sup> increased linearly with sample activity for each isotope. The curves started with 50 Bq and went up to 372 Bq; all readings were above background levels, and all data was adjusted to account for background. The response of the films to the samples was not normalized to the desired sample activities, leading to a wider range of activities used in plotting the calibration curves. In addition, a brief study indicated that the wrinkles present in many samples had no noticeable effect on the film response at the included activity levels.

### 5.3 Filter Analysis

The sample sets on Eichrom Resolve® filters led to higher DLU/mm<sup>2</sup> across all other tested parameters. Cellulose nitrate and Nuclepore filters returned similar values lower than those recorded for Resolve® filters.

## 5.4 Film Comparison

Regardless of film type, the response is known to be a function of exposure time. However, for the same amount of exposure time, MS film proved slightly less sensitive than SR film. On average, SR film had DLU/mm<sup>2</sup> values approximately 1.1 times greater than MS, though MS had background readings approximately 3 times greater than those of the SR film. However, the MS film had a smaller variability than the SR film.

## 5.5 Future Work

Continuation of this work should include investigation of additional isotopes, as well as the relationship between the decay energy and mode of an isotope and the intensity recorded as DLUs. Additional isotopes should span a wide array of decay energies and include common natural or artificial isotopes such as Gd-148 or Th-232. In addition, the relationship between exposure time and recorded intensity should be studied and clarified. Investigation into the effect of mixed sources on both film types should also be completed. A characterization of the uncertainty associated with storage phosphor screens and the system used to image them may also be helpful.

Further study should also be conducted on samples which more closely mimic filters taken from air samples. This particular study examined pure isotopes deposited from solution onto clean filters, while air samplers in contaminated areas will have dust and a mixture of isotopes deposited onto the surface. Dust and material present on the surface of the filter may attenuate alpha radiation and thus affect the response characteristics of any device used to examine the filter, while a mixture of isotopes will lead to a different response profile, especially in a storage phosphor film as the response of the film depends both on sample activity and on emitted energy. Deliberately including impurities, based on impurities that air filters commonly

encounter, in the sample solutions would allow for more “true-to-life” calibration curves to be plotted.



## REFERENCES

- Ang, Dan B., et al. “How Does Signal Fade on Photo-Stimulable Storage Phosphor Imaging Plates When Scanned with a Delay and What Is the Effect on Image Quality?” *Oral Surgery, Oral Medicine, Oral Pathology, Oral Radiology, and Endodontology*, vol. 102, no. 5, 2006, pp. 673–679., doi:10.1016/j.tripleo.2005.11.002.
- Cember, Herman, and Thomas E. Johnson. *Introduction to Health Physics*. 4th. San Francisco: The McGraw-Hill Companies, 2009.
- Charles, M W, and J D Harrison. “Hot Particle Dosimetry and Radiobiology—Past and Present.” *Journal of Radiological Protection*, vol. 27, no. 3A, 2007, doi:10.1088/0952-4746/27/3a/s11.
- Cole, Jennifer M, et al. “Phosphor Imaging as a Tool for in Situ Mapping of Ppm Levels of Uranium and Thorium in Rocks and Minerals.” *Chemical Geology*, vol. 193, no. 1-2, 2003, pp. 127–136., doi:10.1016/s0009-2541(02)00223-1.
- Darley, P.J., et al. “Origins and Dosimetry of 'Hot Particles' from Nuclear Plant Operation.” *Radiation Protection Dosimetry*, vol. 92, no. 1, 2000, pp. 131–137., doi:10.1093/oxfordjournals.rpd.a033258.
- Deresch, A., et al. “Spectral Characterization of Storage Phosphor Imaging Plates.” *AIP Conference Proceedings*, 1581, 2014, pp. 1786–1792., doi:10.1063/1.4865040.
- Eisenbud, Merrill, and Thomas Gesell. *Environmental Radioactivity*. 4th. San Diego: Academic Press, 1997.

- Fichet, Pascal, et al. "Tritium Analysis in Building Dismantling Process Using Digital Autoradiography." *Journal of Radioanalytical and Nuclear Chemistry*, vol. 291, no. 3, 20 Sept. 2011, pp. 869–875., doi:10.1007/s10967-011-1423-1.
- Gallardo, Athena. Investigation of Storage-Phosphor Autoradiography for the Rapid Quantitative Screening of Air filters for Emergency Response Purposes. MS Thesis. University of Nevada, Las Vegas, 2013.
- ICRP. "Radionuclide Transformations - Energy and Intensity of Emissions." ICRP Publication 38, 1983.
- Johnston, R.F., Pickett, S.C., Barker, D.L., 1990. Autoradiography using storage phosphor technology. *Electrophoresis* 11 (5), 355– 360.
- Johnström, Peter, and Anthony P. Davenport. "Imaging and Characterization of Radioligands for Positron Emission Tomography Using Quantitative Phosphor Imaging Autoradiography." *Receptor Binding Techniques*, vol. 897, 2012, pp. 205–220., doi:10.1385/1-59259-927-3:203.
- Knol, Remco J.J., et al. "In Vitro and Ex Vivo Storage Phosphor Imaging of Short-Living Radioisotopes." *Journal of Neuroscience Methods*, vol. 168, no. 2, 15 Mar. 2008, pp. 341–357., doi:10.1016/j.jneumeth.2007.10.028.
- Knoll, Glenn F. *Radiation Detection and Measurement*. 3rd. New York: John Wiley & Sons, Inc., 2000
- Leskinen, Anumaija, et al. "Digital Autoradiography (DA) in Quantification of Trace Level Beta Emitters on Concrete." *Journal of Radioanalytical and Nuclear Chemistry*, vol. 298, no. 1, 16 May 2013, pp. 153–161., doi:10.1007/s10967-013-2535-6.

- Molteni, Roberto. "Effect of Visible Light on Photo-Stimulated-Phosphor Imaging Plates." *International Congress Series*, vol. 1256, 2003, pp. 1199–1205., doi:10.1016/s0531-5131(03)00345-5.
- Mori, Chizuo, et al. "Detection of Extremely Low Level Radioactivity with Imaging Plate." *Nuclear Instruments and Methods in Physics Research A*, no.339 (1994): 278-281
- Parsons-Davis, Tashi, et al. "Application of Modern Autoradiography to Nuclear Forensic Analysis." *Forensic Science International*, vol. 286, Mar. 2018, pp. 223–232., doi:10.1016/j.forsciint.2018.03.027.
- Perkin Elmer Inc. *Cyclone Plus Storage Phosphor System Operation Manual*. Downers Grove: Perkin Elmer Inc., 2006.
- Perkin Elmer Inc. *Cyclone Plus Storage Phosphor System: Specifications*. Shelton: Perkin Elmer Inc., 2006.
- Perkin Elmer Inc. *OptiQuant Image Analysis Software Reference*. Downers Grove: Perkin Elmer Inc., 2006.
- Upham, L.V., Englert, D.F., 1998. Radionuclide imaging. In: L'Annunziata, M.F. (Ed.), *Handbook of Radioactivity Analysis*. Academic Press, New York, pp. 647– 692.
- Weissman, L, et al. "Beam Profile Measurements with a Phosphor Imaging Plate." *Nuclear Instruments and Methods in Physics Research Section A: Accelerators, Spectrometers, Detectors and Associated Equipment*, vol. 400, no. 2-3, 1997, pp. 409–413., doi:10.1016/s0168-9002(97)81491-x.
- Yagoda, Herman. *Radioactive Measurements with Nuclear Emulsions*. New York: John Wiley & Sons, Inc., 1949

## APPENDIX A

### A.1. Equipment

- Filter apparatus (PAL Lifescience apparatus with polycarbonate base and metal screen, 25 mm polysulfone funnel and 250 mL polypropylene flask)
- Filters
  - Eichrom Resolve® 0.1 µm polypropylene
  - Whatman™ Nuclepore Track-Etch Membrane, 0.1 µm
  - Whatman™ Cellulose Nitrate Membrane Filters, 0.1 µm
- Centrifuge tubes (15 mL)
- Petri dishes
- Stainless steel planchets (100)
- Automatic pipette (0.02 – 0.2 mL and 0.1 – 1.0 mL)
- Teflon coated tweezers
- Double sided tape

### A.2. Chemicals & Radionuclides

- Cerium nitrate ( $\text{Ce}(\text{NO}_3)_3$ ) solution ( $0.5 \text{ mg mL}^{-1} \text{ Ce}$ )
- Hydrofluoric acid (concentrated)
- Nitric acid (0.1 M)
- Ethanol solution (80% v/v)
- Plutonium-239 stock solution (1000 Bq/mL in 0.1 M  $\text{HNO}_3$ )
- Americium-241 stock solution (1000 Bq/mL in 0.1 M  $\text{HNO}_3$ )
- Curium-244 stock solution (1000 Bq/mL in 0.1 M  $\text{HNO}_3$ )

## APPENDIX B

Figure 16- OptiQuant software protocol prior to scanning. and Figure 17- OptiQuant software protocol prior to generating the report output on one of the screens. show the protocols used to gather data using the OptiQuant software.

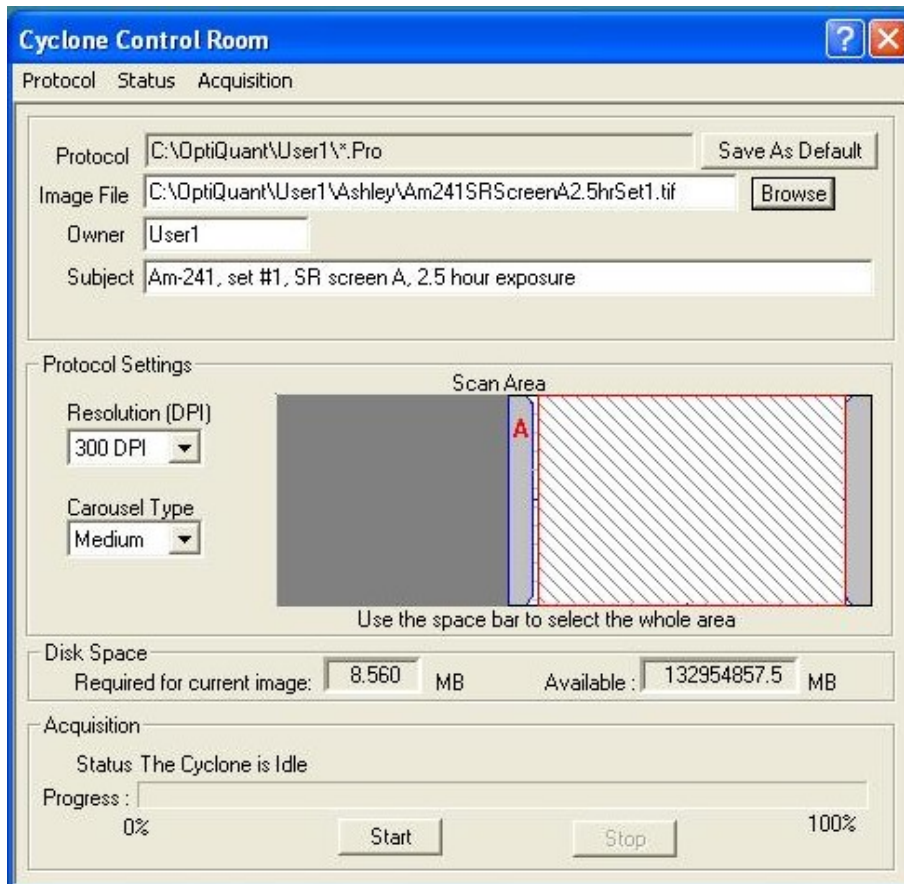


Figure 16- OptiQuant software protocol prior to scanning.

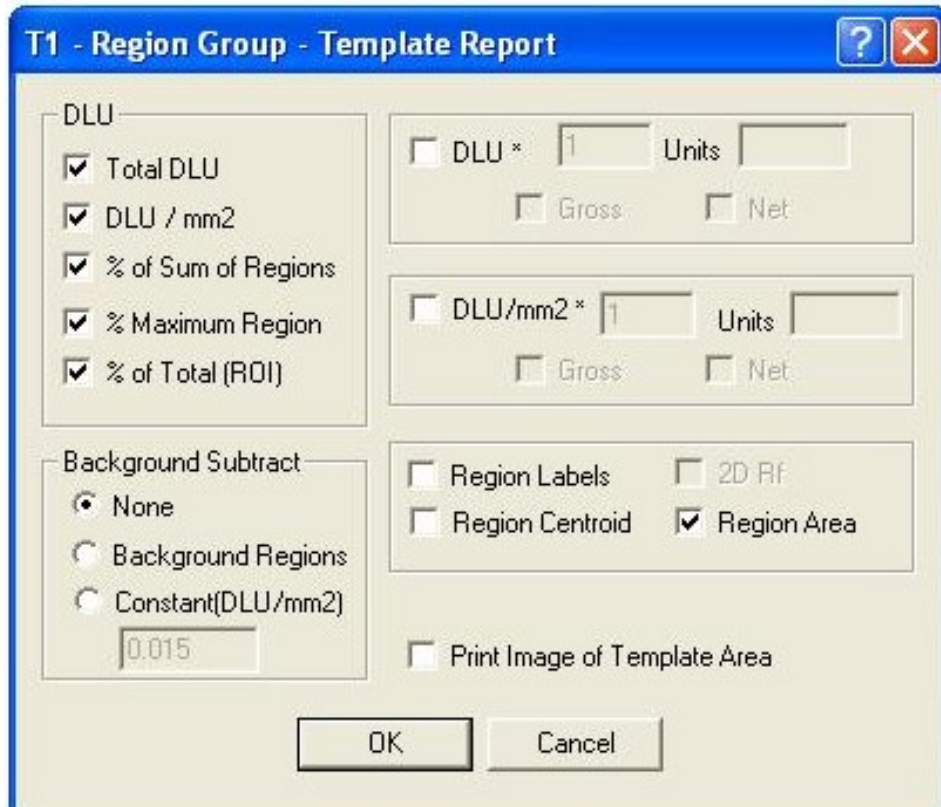


Figure 17- OptiQuant software protocol prior to generating the report output on one of the screens.

## APPENDIX C

Raw data for figures.

*Table 6- Raw data for Figures 4, 8, and 10.*

Isotope	Set	Desired Activity (Bq)	Actual Activity (Bq)	DLU/mm <sup>2</sup>	Area mm <sup>2</sup>	DLU/mm <sup>2</sup> adjusted for background
Pu239	1	50	67.04774	79846.2	490.9	79501.5
		100	134.3797	162010.9	490.9	161666.2
		150	165.785	233251.8	490.9	232907.1
		200	264.6866	307055.7	490.9	306711.0
		250	322.0252	341744.8	490.9	341400.1
	2	50	63.08601	71649.5	490.9	71304.8
		100	136.2447	148153.1	490.9	147808.4
		150	218.4859	235077.6	490.9	234732.9
		200	286.8307	287873.1	490.9	287528.4
		250	372.3617	419032.0	490.9	418687.3
	3	50	65.54266	72437.9	490.9	72093.2
		100	142.82	150489.4	490.9	150144.7
		150	199.8025	206702.0	490.9	206357.3
		200	274.5965	285958.3	490.9	285613.6
		250	349.9043	382073.0	490.9	381728.3
	S	50	63.08601	71265.3	490.9	70920.6
		100	136.2447	154071.2	490.9	153726.5
		150	165.785	219320.7	490.9	218976.0
		200	264.6866	288146.6	490.9	287801.9
		250	322.0252	360296.2	490.9	359951.5

Table 7- Raw data for Figures 7 and 10.

Isotope	Set	Desired Activity (Bq)	Actual Activity (Bq)	DLU/mm <sup>2</sup>	Area mm <sup>2</sup>	DLU/mm <sup>2</sup> adjusted for background
Am241	1	50	55.52353	93633.6	490.9	93328.8
		100	113.4669	184760.5	490.9	184455.7
		150	172.4292	279888.1	490.9	279583.3
		200	226.3863	371095.0	490.9	370790.2
		250	289.0533	447134.6	490.9	446829.8
	2	50	55.8896	76270.2	490.9	75965.4
		100	113.1133	150761.2	490.9	150456.4
		150	172.487	212481.5	490.9	212176.7
		200	224.8558	299403.9	490.9	299099.1
		250	295.7646	389752.3	490.9	389447.5
	3	50	61.07765	70231.7	490.9	69926.9
		100	119.4373	150757.9	490.9	150453.1
		150	182.5451	203420.5	490.9	203115.7
		200	249.2736	280911.6	490.9	280606.8
		250	301.3465	388881.8	490.9	388577.0

Table 8- Raw data for Figures 9 and 10.

Isotope	Set	Desired Activity (Bq)	Actual Activity (Bq)	DLU/mm <sup>2</sup>	Area mm <sup>2</sup>	DLU/mm <sup>2</sup> adjusted for background
Cm244	1	50	54.03567	91729.1	490.9	91424.3
		100	110.3196	188959.7	490.9	188654.9
		150	165.6795	288487.8	490.9	288183.0
		200	219.0739	384128.6	490.9	383823.8
		250	273.7172	477094.2	490.9	476789.4
	2	50	55.65355	84135.8	490.9	83831.0
		100	115.7325	164362.6	490.9	164057.8
		150	175.7505	325737.6	490.9	325432.8
		200	230.3202	251881.0	490.9	251576.2
		250	270.5996	417087.0	490.9	416782.2
	3	50	56.15847	76599.0	490.9	76254.3
		100	114.5302	164047.3	490.9	163702.6
		150	170.0175	225053.5	490.9	224708.8
		200	218.8326	303777.3	490.9	303432.6
		250	273.9554	370809.6	490.9	370464.9



Table 9- Raw data for Figure 11.

Isotope	Set	Activity (Bq)	Actual activity (Bq)	DLU/mm <sup>2</sup>	Area mm <sup>2</sup>	DLU/mm <sup>2</sup> adjusted for background
Am241	1	50	55.52353	68637.2	490.9	67576.1
		100	113.4669	143392.2	490.9	142331.1
		150	172.4292	201647.5	490.9	200586.4
		200	226.3863	280984.1	490.9	279923.0
		250	289.0533	352022.4	490.9	350961.3
	2	50	55.8896	65076.3	490.9	64015.2
		100	113.1133	138784.0	490.9	137722.9
		150	172.487	204215.0	490.9	203153.9
		200	224.8558	274470.9	490.9	273409.8
		250	295.7646	358338.6	490.9	357277.5
	3	50	61.07765	72759.3	490.9	71698.2
		100	119.4373	143440.0	490.9	142378.9
		150	182.5451	216113.5	490.9	215052.4
		200	249.2736	287504.8	490.9	286443.7
		250	301.3465	364985.3	490.9	363924.2
Pu239	1	50	67.04774	65714.6	490.9	64616.7
		100	134.3797	133579.0	490.9	132481.1
		150	165.785	191447.3	490.9	190349.4
		200	264.6866	259807.2	490.9	258709.3
		250	322.0252	318563.2	490.9	317465.3
	2	50	63.08601	58008.3	490.9	56910.4
		100	136.2447	128709.9	490.9	127612.0
		150	218.4859	199850.1	490.9	198752.2
		200	286.8307	261912.0	490.9	260814.1
		250	372.3617	348044.5	490.9	346946.6
	3	50	65.54266	62964.1	490.9	61866.2
		100	142.82	136362.6	490.9	135264.7
		150	199.8025	186505.1	490.9	185407.2
		200	274.5965	261912.2	490.9	260814.3
		250	349.9043	326177.7	490.9	325079.8
Cm244	1	50	54.03567	73798.4	490.9	72737.3
		100	110.3196	150507.7	490.9	149446.6
		150	165.6795	219333.8	490.9	218272.7
		200	219.0739	303524.4	490.9	302463.3
		250	273.7172	380940.0	490.9	379878.9
	2	50	55.65355	77526.6	490.9	76428.7

		100	115.7325	163651.5	490.9	162553.6
		150	175.7505	241885.4	490.9	240787.5
		200	230.3202	324344.6	490.9	323246.7
		250	270.5996	381302.4	490.9	380204.5
	3	50	56.15847	73761.5	490.9	72700.4
		100	114.5302	148538.4	490.9	147477.3
		150	170.0175	212384.1	490.9	211323.0
		200	218.8326	276623.5	490.9	275562.4
		250	273.9554	349720.1	490.9	348659.0

Table 10- Raw data for Figure 12.

Isotope	Set	Desired Activity (Bq)	Actual Activity (Bq)	DLU/mm <sup>2</sup>	Area mm <sup>2</sup>	DLU/mm <sup>2</sup> adjusted for background	Normalized activities (Bq)
Am241	Nuclepore	150.0	145.0	196052.8	490.9	195713.0	202398.6
Am241	Nuclepore	150.0	154.4	184697.3	490.9	184357.5	179078.3
Am241	Nuclepore	150.0	165.1	199102.3	490.9	198762.5	180618.9
		Average			490.9	192944.3	187365.3
Am241	Cellulose nitrate	150.0	189.1	238245.5	490.9	237905.7	188702.1
Am241	Cellulose nitrate	150.0	184.2	228610.9	490.9	228271.1	185915.4
Am241	Cellulose nitrate	150.0	182.1	219393.1	490.9	219053.3	180481.0
		Average			490.9	228410.0	185032.8
Pu239	Nuclepore	150.0	203.5	211533.7	490.9	117900.1	86925.5
Pu239	Nuclepore	150.0	191.0	209954.1	490.9	116320.5	91374.2
Pu239	Nuclepore	150.0	189.9	191320.0	490.9	97686.4	77154.4
		Average			490.9	110635.7	85151.4
Pu239	Cellulose nitrate	150.0	208.8	217670.5	490.9	124036.9	89102.7
Pu239	Cellulose nitrate	150.0	210.4	222612.6	490.9	128979.0	91960.3
Pu239	Cellulose nitrate	150.0	209.6	221200.9	490.9	127567.3	91309.2
		Average			490.9	126861.1	90790.7
Cm244	Nuclepore	150.0	159.7	219448.1	490.9	219108.3	205775.9
Cm244	Nuclepore	150.0	157.7	214861.7	490.9	214521.9	204056.4
Cm244	Nuclepore	150.0	157.3	214575.0	490.9	214235.2	204242.5
		Average			490.9	215955.1	204691.6
Cm244	Cellulose nitrate	150.0	168.4	232160.9	490.9	231821.1	206515.5
Cm244	Cellulose nitrate	150.0	169.1	213585.3	490.9	213245.5	189193.7
Cm244	Cellulose nitrate	150.0	164.3	246188.3	490.9	245848.5	224498.8
		Average			490.9	230305.0	206736.0

Table 11- Raw data for Figure 13.

Isotope	Set	Activity (Bq)	Actual activity (Bq)	DLU/mm <sup>2</sup>	Area mm <sup>2</sup>	DLU/mm <sup>2</sup> adjusted for background	Normalized activities (Bq)
Am241	Nuclepore	150	145.0452	163423.4	490.9	162362.3	167908.7
Am241	Nuclepore	150	154.422	170900.8	490.9	169839.7	164976.3
Am241	Nuclepore	150	165.0678	175978.4	490.9	174917.3	158950.4
		Average			490.9	169039.8	163945.1
Am241	Cellulose nitrate	150	189.1121	208607.8	490.9	207546.7	164622.0
Am241	Cellulose nitrate	150	184.1734	204345	490.9	203283.9	165564.6
Am241	Cellulose nitrate	150	182.058	199913.8	490.9	198852.7	163837.4
		Average			490.9	203227.8	164674.7
Pu239	Nuclepore	150	203.4503	174350.9	490.9	173253	127736.1
Pu239	Nuclepore	150	190.9518	169731.4	490.9	168633.5	132468.1
Pu239	Nuclepore	150	189.9173	159547.6	490.9	158449.7	125146.3
		Average			490.9	166778.7	128450.2
Pu239	Cellulose nitrate	150	208.8099	180608.8	490.9	179510.9	128952.8
Pu239	Cellulose nitrate	150	210.3827	191614.4	490.9	190516.5	135835.6
Pu239	Cellulose nitrate	150	209.5638	184087.9	490.9	182990	130979.2
		Average			490.9	184339.1	131922.6
Cm244	Nuclepore	150	159.7187	202684.3	490.9	201623.2	189354.7
Cm244	Nuclepore	150	157.6931	207564.4	490.9	206503.3	196429.0
Cm244	Nuclepore	150	157.3388	201957.5	490.9	200896.4	191525.9
		Average			490.9	203007.7	192436.6
Cm244	Cellulose nitrate	150	168.3804	232721	490.9	231659.9	206371.9
Cm244	Cellulose nitrate	150	169.0692	227087.8	490.9	226026.7	200533.3
Cm244	Cellulose nitrate	150	164.2649	222140.4	490.9	221079.3	201880.6
		Average			490.9	226255.3	202928.6

## CURRICULUM VITAE

Ashley Sorcic

3108 Swallow Place

Fort Collins, CO 80525

240-507-2914

asorcic@hotmail.com

### **Education**

Master of Science, Health Physics, Colorado State University, GPA: 4.0/4.0, May 2019

Bachelor of Science, Engineering, Southern Utah University, GPA: 3.4/4.0, April 2017

### **Work Experience**

Summer and December 2018 Student Trainee, Naval Weapons Station Yorktown RADIAC

Responsible for pre- and post-checks on alpha detectors, open-air neutron measurements, assisting calculations of anisotropy factors for a neutron source, and writing a standard operating procedure for a piece of equipment.

Summer 2017 Graduate Research Aide, Argonne National Laboratory

Compared the recovery of barium from strontium resin for various chelating agents at several pH levels and concentrations, to improve age-dating methods for cesium sources.

January 2017 – April 2017 Teacher's Aide, Southern Utah University

Responsible for grading student work in ENGR 4300 – Vibrations.

September 2015 – May 2016 Writing Fellow, Southern Utah University

Responsible for tutoring 28 students in ENGR 2140 – Strength of Materials to improve technical writing skills.

Summer 2014 & 2015 Customer Service Representative, Hobby Lobby

Responsible for cash transactions in excess of \$1000 per day and assisting customers.

### **Presentations**

Sorcic AK, McLain DR. *The Effects of Chelating Agents on Recovering Barium from Sr Resin.*

Health Physics Society Midyear meeting, January 2018

Sorcic AK, McLain DR. *Comparison of the Effects of chelating Agents on Recovery of Barium from Strontium Resin.* Methods and Applications of Radioanalytical Chemistry (MARC) XI meeting, April 2018

Sorcic AK, McLain DR, Sudowe R. *Recovering barium from strontium resin using chelating agents.* American Chemical Society (ACS) 255<sup>th</sup> National Meeting, March 2018

### **Awards and Scholarships**

Dean's list, SUU, College of Science and Engineering, Fall 2015

AMPAC Scholarship, SUU, Fall 2016 & Spring 2017

Walter Maxwell Gibson Scholarship, SUU, Fall 2015 & Spring 2016

Juergen H Staudte Scholarship, SUU, Fall 2015 & Spring 2016

SUU President's Non-Resident Scholarship, Fall 2013 – Spring 2015

### **Relevant Computer Experience**

Monte Carlo N-Particle Transport Code (MCNP)

Microsoft Office: Word, Excel, Powerpoint

Matlab: Basic functions and coding, Simulink, Root locus design

SolidWorks: 3-D modeling

### **Professional Service and Volunteer Work**

September 2016 – April 2017 **Southwest Wildlife Foundation Visitor's Center**. Responsible for researching the viability of geothermal climate-control technology in the specific case of the proposed visitor's center, calculating the system specifications necessary should the SWF install a geothermal system, and double-checking load calculations from the structural design analysis team.

May 2016 **Southern Utah University Writing Center**. Responsible, with three other students, for tutoring Chinese students attending Wuhan Polytechnic University in Wuhan, China, in writing English-language essays and aiding the associated professor while she taught writing classes.